

# Resistive Memory based Efficient Machine Unlearning and Continual Learning

Ning Lin<sup>1,2,9</sup>, Jichang Yang<sup>1,2,4,9</sup>, Yangu He<sup>1,2,4,9</sup>, Zijian Ye<sup>1</sup>, Kwun Hang Wong<sup>1</sup>, Xinyuan Zhang<sup>1,4</sup>, Songqi Wang<sup>1,4</sup>, Yi Li<sup>1,4</sup>, Kemi Xu<sup>7,8</sup>, Leo Yu Zhang<sup>6</sup>, Xiaoming Chen<sup>5</sup>, Dashan Shang<sup>3</sup>, Han Wang<sup>1,\*</sup>, Xiaojuan Qi<sup>1,\*</sup>, and Zhongrui Wang<sup>2,\*</sup>

<sup>1</sup>Department of Electrical and Electronic Engineering, the University of Hong Kong, Hong Kong, China

<sup>2</sup>The School of Microelectronics, Southern University of Science and Technology, Shenzhen 518055, China

<sup>3</sup>Institute of Microelectronics, Chinese Academy of Sciences, Beijing 100029, China

<sup>4</sup>Centre for Advanced Semiconductors and Integrated Circuits, the University of Hong Kong, Hong Kong, China

<sup>5</sup>Institute of Computing Technology, Chinese Academy of Sciences, Beijing 100190, China

<sup>6</sup>The School of Information and Communication Technology, Griffith University, QLD 4215, Australia

<sup>7</sup>MIIT Key Laboratory of Complex-field Intelligent Sensing, School of Optics and Photonics, Beijing Institute of Technology, Beijing 100081, China

<sup>8</sup>Center for Photonic Quantum Precision Measurement, Advanced Research Institute of Multidisciplinary Science, Beijing Institute of Technology, Beijing 100081, China

<sup>\*</sup>These authors contributed equally.

<sup>\*</sup>e-mail: hanwang6@hku.hk; xjqi@eee.hku.hk; zrwang@eee.hku.hk

## ABSTRACT

Resistive memory (RM) based neuromorphic systems can emulate synaptic plasticity and thus support continual learning, but they generally lack biologically inspired mechanisms for active forgetting, which are critical for meeting modern data privacy requirements. Algorithmic forgetting, or machine unlearning, seeks to remove the influence of specific data from trained models to prevent memorization of sensitive information and the generation of harmful content, yet existing exact and approximate unlearning schemes incur prohibitive programming overheads on RM hardware owing to device variability and iterative write-verify cycles. Analogue implementations of continual learning face similar barriers. Here we present a hardware-software co-design that enables an efficient training, deployment and inference pipeline for machine unlearning and continual learning on RM accelerators. At the software level, we introduce a low-rank adaptation (LoRA) framework that confines updates to compact parameter branches, substantially reducing the number of trainable parameters and therefore the training cost. At the hardware level, we develop a hybrid analogue-digital compute-in-memory system in which well-trained weights are stored in analogue RM arrays, whereas dynamic LoRA updates are implemented in a digital computing unit with SRAM buffer. This hybrid architecture avoids costly reprogramming of analogue weights and maintains high energy efficiency during inference. Fabricated in a 180 nm CMOS process, the prototype achieves up to a 147.76-fold reduction in training cost, a 387.95-fold reduction in deployment overhead and a 48.44-fold reduction in inference energy across privacy-sensitive tasks including face recognition, speaker authentication and stylized image generation, paving the way for secure and efficient neuromorphic intelligence at the edge.

## Introduction

The human brain supports lifelong adaptation while operating at remarkably low power<sup>1</sup>. Two key principles underlie this efficiency. First, biological neural networks effectively implement computation in memory: synapses simultaneously store long-term connection strengths (weights) and perform local weighted transmission of signals, enabling massive parallelism with minimal data movement<sup>2-5</sup>. Second, this lifelong adaptability is mediated by selective plasticity: only a small fraction of synaptic weights is modified in response to new experiences<sup>6</sup>, with connection strengths being locally adjusted rather than globally rewritten. Such sparse, localized plasticity underlies biological analogues of both machine unlearning (active forgetting) and continual learning.

On-device adaptability is increasingly required in modern neuromorphic systems, particularly for edge deployments such as smart cameras, voice assistants and mobile generative applications. However, today's mainstream hardware remains dominated by the von Neumann paradigm, in which memory and computation are physically separated<sup>7</sup>. The resulting data movement between memory and processor incurs substantial energy and latency overheads, creating a fundamental bottleneck

for deploying adaptive intelligence under tight power budgets<sup>8</sup>. Computing-in-memory (CIM) accelerators based on emerging non-volatile resistive memory (RM) devices offer a compelling alternative by co-locating storage and multiply-accumulate operations inside dense crossbar arrays, and have demonstrated high throughput and energy efficiency for inference<sup>9–12</sup>.

Achieving brain-like machine unlearning and continual learning on RM-based accelerators remains challenging. While RM arrays can efficiently host static pretrained weights for inference, reprogramming analogue conductances is costly and unreliable in practice: device stochasticity and variability typically require iterative write-verify cycles to reach target precision, leading to high update energy, long latency and the accumulation of programming errors<sup>13–16</sup>. As a result, many RM neuromorphic systems are effectively inference-centric<sup>9–12</sup>, and the frequent parameter updates needed for on-device machine unlearning and continual learning become prohibitively expensive.

In parallel, the software mechanisms for machine unlearning and continual learning introduce additional mismatches with edge neuromorphic hardware. Machine unlearning<sup>17</sup> is increasingly important for removing the influence of specific data from deployed models<sup>18,19</sup>, for example to erase memorized sensitive identities or to revoke undesired generative behaviours under privacy and safety constraints<sup>20,21</sup>. At the same time, continual learning is needed to incorporate new tasks over time without catastrophic forgetting<sup>22–25</sup>. However, many existing approaches implicitly assume Graphics Processing Unit (GPU)-like platforms with fast, precise and low-cost parameter updates, and commonly rely on replay buffers and/or modifying large portions of the network. These strategies do not map well to analogue CIM accelerators, where frequent large-scale model reprogramming is a dominant cost.

Here we propose a hardware-software co-design that enables efficient machine unlearning and continual learning on RM-based CIM accelerators. On the hardware side, we introduce a hybrid analogue-digital CIM system: analogue RM crossbars provide non-volatile, high-density storage for pretrained backbone weights, whereas digital computing unit with SRAM buffer supports fast, energy-efficient and accurate updates for lightweight adaptation branches. On the software side, we develop a low-rank adaptation (LoRA)-based framework<sup>26</sup> that confines machine unlearning and continual learning to compact low-rank parameter updates, so that only the SRAM-resident LoRA weights are modified during deployment, avoiding costly reprogramming of the analogue RM arrays.

We experimentally validate the proposed framework on a fabricated RM-based CIM macro, across three privacy-sensitive applications: face identification (ID) recognition, speaker authentication and stylized image generation. Across these tasks, the hybrid architecture combined with LoRA-based adaptation achieves substantially lower training cost (approximately  $25.16 \times$ – $147.76 \times$  reduction), significantly reduced on-chip deployment cost (approximately  $63.74 \times$ – $387.95 \times$  reduction) and markedly lower inference energy (approximately  $6.13 \times$ – $48.44 \times$  reduction), while preserving competitive accuracy. These results provide a practical pathway towards secure and efficient neuromorphic intelligence at the edge.

## Results

### Hardware-Software Co-Design

Fig. 1 summarises the hardware-software co-design that enables LoRA-based machine unlearning and continual learning on a hybrid analogue-digital platform. In realistic edge deployments, models on devices such as smart cameras cannot remain static: they must adapt to changing environments by removing the influence of sensitive data to comply with privacy and safety regulations, and by incorporating new data over time (Fig. 1a). In the hippocampus, a brain region central to memory formation, synaptic connections are strengthened during learning and gradually weakened during forgetting (Fig. 1b). RM crossbars similarly integrate storage and computation, but they lack an intrinsic mechanism for controlled forgetting.

To address this gap, we develop a hardware-software co-design that emulates hippocampal-like dynamics in RM-based CIM systems using digital LoRA branches (Fig. 1c). At the software level, LoRA-based adaptation confines machine unlearning and continual learning to a small set of low-rank parameters that are updated in response to environmental shifts, thereby reducing training overhead. At the hardware level, a hybrid analogue-digital design stores static pretrained weights in analogue RM crossbars, while adaptive LoRA weights reside in SRAM and are processed by a digital compute unit. During deployment, only the SRAM-resident LoRA weights are updated, avoiding reprogramming of the analogue RM arrays and substantially reducing RM programming cost.

Fig. 2a presents, from left to right, a photograph of a  $32 \times 32$  1-transistor-1-resistor (1T1R) chip, optical micrographs of the RM array, a transmission electron microscopy (TEM) image of a 1T1R cell, and TEM images of the TiN/Ta<sub>2</sub>O<sub>5</sub>/TaO<sub>x</sub>/TiN RM stack. Panels (b)–(f) of Fig. 2 summarise the electrical characteristics and multilevel read/write capabilities of the RM devices. Quasi-static  $I$ – $V$  sweeps over 50 cycles (Fig. 2b) exhibit highly uniform bipolar resistive switching. Robust endurance is observed over 30,000 cycles of SET and RESET operations (Fig. 2c). Single-shot SET programming yields more than 128 approximately linearly spaced conductance levels (Fig. 2d), demonstrating the strong multilevel capability of the RM cells. Repeated readout of 17 RM cells with distinct conductance levels (Fig. 2e) demonstrates stable programmed conductances over  $10^6$  s, with minimal temporal fluctuations and read noise, indicating excellent read stability. Fig. 2f shows programming trajectories for four RM cells targeting distinct conductance values, each requiring tens of operations.

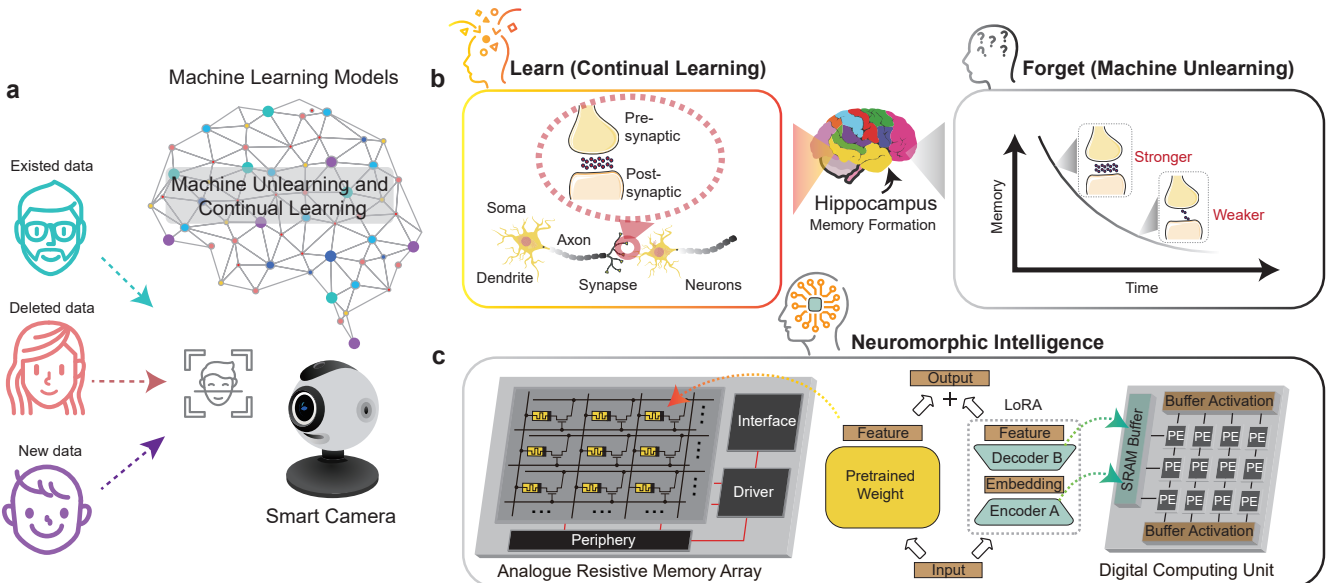


**Figure 1. Hardware-software co-design for LoRA-based machine unlearning and continual learning on a hybrid analogue-digital system.** **a**, Machine learning models deployed on edge devices (for example, smart cameras) must support machine unlearning and continual learning to remove the influence of sensitive information contained in deleted data and to continually acquire knowledge from new data over time. **b**, Schematic of hippocampal synaptic plasticity. The hippocampus, a brain region central to memory formation, supports both learning and forgetting: during learning, synaptic transmission between pre- and postsynaptic neurons is strengthened, whereas over time this connection weakens, facilitating natural unlearning. **c**, Conceptual diagram of the proposed hardware-software co-design. The hybrid architecture combines analogue RM crossbar arrays, which store static pretrained backbone weights, with a digital compute unit incorporating an SRAM buffer that hosts lightweight LoRA branches for on-device machine unlearning and continual learning.

Panels (g)-(h) of Fig. 2 highlight the challenges inherent in RM programming. In Fig. 2g, target conductance maps encoding the 'CL' (continual learning) and 'UL' (machine unlearning) patterns are programmed using a halting criterion that stops the write operation when the programming error is within a  $2 \mu\text{S}$  tolerance, resulting in only a small residual conductance error and programmed maps that closely match the targets. Achieving this precision, however, requires iterative tuning. Fig. 2h quantifies this trade-off by plotting the mean number of programming cycles per cell against the conductance error (shaded area, standard deviation); higher precision demands substantially more iterations. For example, achieving an error below  $1 \mu\text{S}$  requires approximately 50 cycles per cell on average.

## Face Recognition

Face recognition in smart cameras raises acute privacy concerns and demands strict data protection. After deployment, models must adapt to personnel turnover by adding or removing identities in the recognition database, while the underlying model must be updated by machine unlearning and continual learning to remain effective. We demonstrate these processes on face-recognition tasks using a LoRA-enabled RM analogue-digital system on the Olivetti faces dataset<sup>27</sup>.

Fig. 3a-c illustrate the model architecture and parameter transformations during learning, machine unlearning and continual learning. Fig. 3a shows the MLP-Mixer architecture<sup>28</sup>, which consists of per-patch multilayer perceptrons (MLPs), mixer layers and an output layer, all implemented with fully connected layers (see Supplementary Fig. 1 for details). During initial learning, pretrained weights are programmed into the RM analogue array. The resulting conductance maps of the patch MLPs, mixer layer and output layer are shown in Fig. 3a, with conductance values ranging from  $10 \mu\text{S}$  to  $80 \mu\text{S}$ . To mitigate RM programming overhead, subsequent machine unlearning of face ID 2 (Fig. 3b) and continual learning of face ID 5 (Fig. 3c) are performed by updating only the encoder and decoder parameters of the LoRA modules.

Fig. 3d-f track the evolution of the representation space and recognition performance. Two-dimensional t-distributed stochastic neighbour embedding (t-SNE) visualizations of the embedding space reveal dynamic reconfiguration across the three stages. After initial learning, embeddings from five face classes form well-separated clusters, indicating accurate recognition (Fig. 3d). After unlearning face ID 2 via gradient ascent, features of the second class (green) overlap with those of the fourth class (blue), indicating loss of discriminative power for the second identity (Fig. 3e). Subsequent continual learning of a new

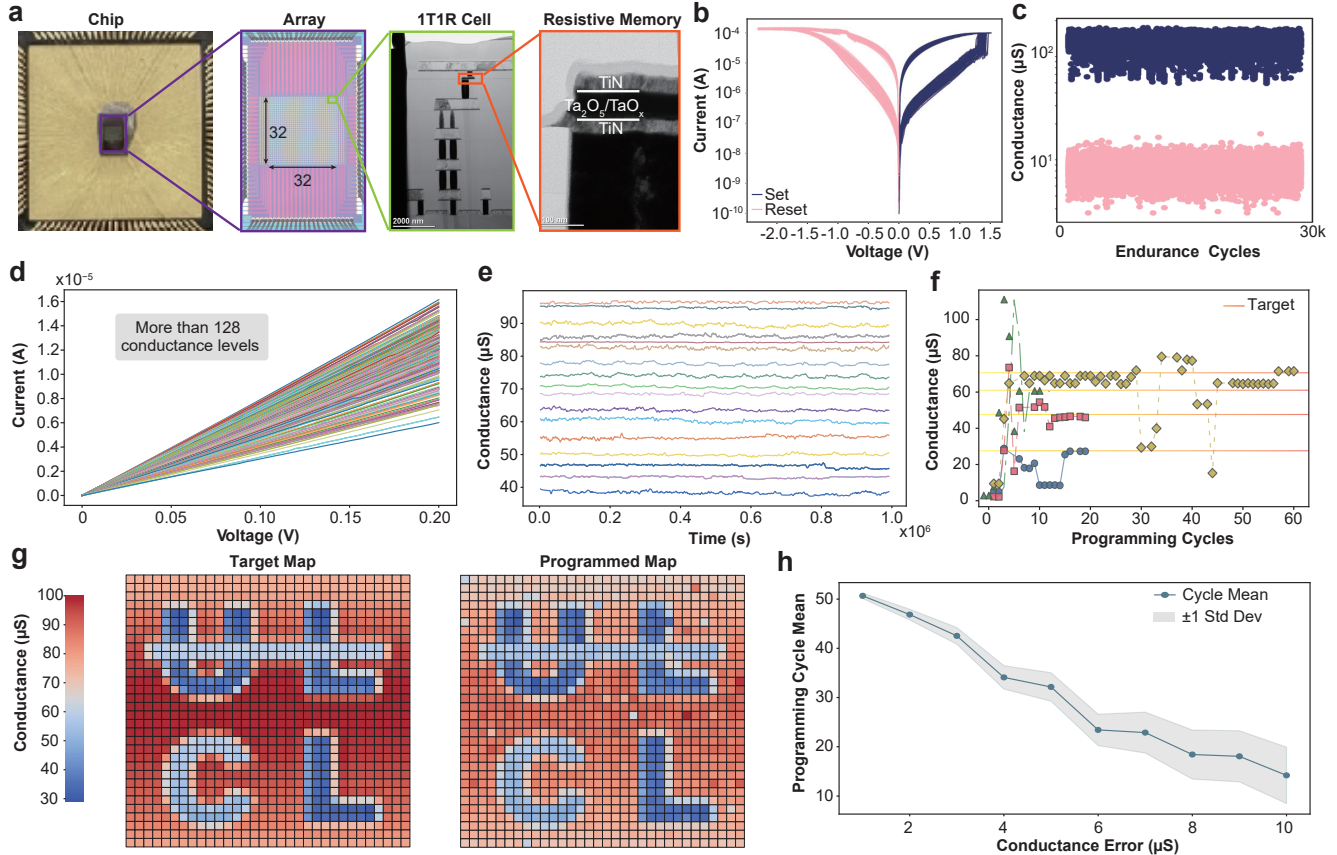


**Figure 2. Hybrid analogue-digital architecture and RM device characteristics for programming.** **a**, Photograph of a 32 × 32 1T1R chip, optical micrograph of the RM array, and cross-sectional transmission electron microscopy (TEM) images of a 1-transistor-1-resistor (1T1R) cell and the RM stack. **b**, Quasi-static  $I$ - $V$  sweeps of an RM cell over 50 cycles, showing repeatable bipolar resistive switching. **c**, Endurance of an RM cell over 30,000 SET/RESET cycles. **d**, Single-shot SET programming of an RM cell into more than 128 conductance levels by varying the programming voltage. **e**, Time evolution of the programmed conductance over  $10^6$  s, demonstrating stable readout. **f**, Programming trajectories for four RM cells with conductances tuned towards different target values. **g**, Target and programmed conductance maps encoding ‘UL’ (machine unlearning) and ‘CL’ (continual learning), programmed using a halting criterion that stops the write operation when the programming error is within a  $2\ \mu\text{S}$  tolerance. **h**, Relationship between the number of programming cycles per cell and the conductance error after programming (solid line, mean; shaded area, standard deviation).

face ID 5 using a replay strategy produces a new cluster that remains well separated from existing identities, demonstrating robust adaptability without catastrophic forgetting (Fig. 3f).

Fig. 3g highlights the benefits of the proposed hardware-software co-design by comparing inference accuracy obtained with fully analogue RM parameter updates and with the RM with digital LoRA accelerator (RM-DLoRA). The hybrid architecture achieves higher accuracy because it avoids repeated, error-prone analogue reprogramming, thereby reducing cumulative programming noise during inference after initial learning, machine unlearning (UL) and continual learning (CL) (see Supplementary Fig. 2 for the noise tolerance of RM programming).

A quantitative comparison of the three core workflows of training, deployment and inference is summarized in Fig. 3h-j. Fig. 3h shows that RM-DLoRA requires substantially lower training cost than conventional full-parameter fine-tuning on RM, reducing training update cost by  $36.68\times$  and  $27.51\times$  for UL and CL, respectively. Fig. 3i quantifies write overhead during deployment. Whereas traditional RM program updates require repeated analogue reprogramming of RM arrays, RM-DLoRA updates only the LoRA weights stored in SRAM, reducing write-energy consumption by  $92.91\times$  and  $69.68\times$  for UL and CL, respectively. As shown in Fig. 3j, RM-DLoRA further improves energy efficiency during inference procedure, achieving  $20.19\times$ ,  $25.43\times$  and  $12.48\times$  lower energy consumption than a GPU for learn, UL and CL, respectively.

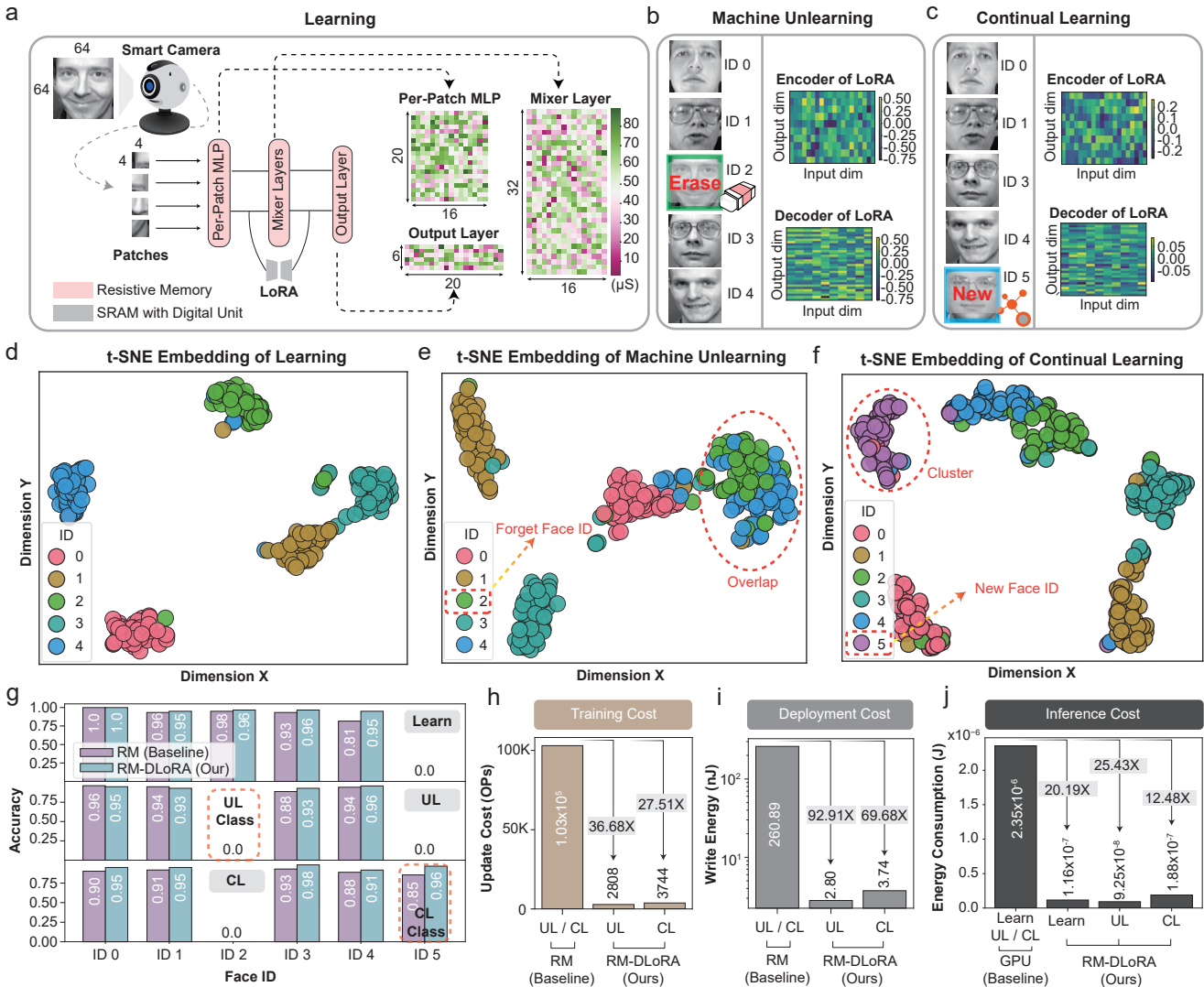


**Figure 3. Learning, machine unlearning (UL) and continual learning (CL) for face classification on the Olivetti faces dataset.** **a**, Schematic of the MLP-Mixer architecture mapped onto RM array for initial learning. **b**, Machine unlearning of face ID 2 using exemplar LoRA encoder and decoder modules. **c**, Continual learning of face ID 5 using exemplar LoRA encoder and decoder modules. **d-f**, Two-dimensional t-distributed stochastic neighbour embedding (t-SNE) visualizations of the embedding space after learning (**d**), machine unlearning (**e**) and continual learning (**f**). **g**, Classification accuracy obtained with the our hybrid RM with digital LoRA architecture (RM-DLoRA) and with fully analogue RM reprogramming baseline method, showing higher accuracy for RM-DLoRA owing to the avoidance of repeated analogue reprogramming in learn, machine unlearning (UL) and continual learning (CL) tasks. **h**, Training update cost for full-parameter fine-tuning on RM and RM-DLoRA, our method reducing training cost by about  $36.68\times$  and  $27.15\times$  in UL and CL tasks. **i**, Write-energy consumption for full-parameter fine-tuning on RM and RM-DLoRA, our method reducing write energy by about  $92.91\times$  and  $69.68\times$  in UL and CL tasks. **j**, Inference energy for RM-DLoRA and a GPU baseline, with RM-DLoRA achieving about  $20.19\times$ ,  $25.43\times$  and  $12.48\times$  lower energy consumption in learning (Learn), UL and CL tasks.

## Speaker Authentication

Speaker authentication is widely integrated into voice assistants on smart speakers to authenticate users and control smart home devices (Fig. 4a). In such applications, enrolling new users and removing existing ones is routine. The ability to make the model effectively “forget” a specific user’s voice is crucial for privacy protection. This ensures that a forgotten speaker cannot be identified, even if the model or its parameters are accessed by a third party. Conversely, when enrolling a new authorized user, the system must retain sufficient capacity to learn the new voice without degrading recognition accuracy for previously registered users.

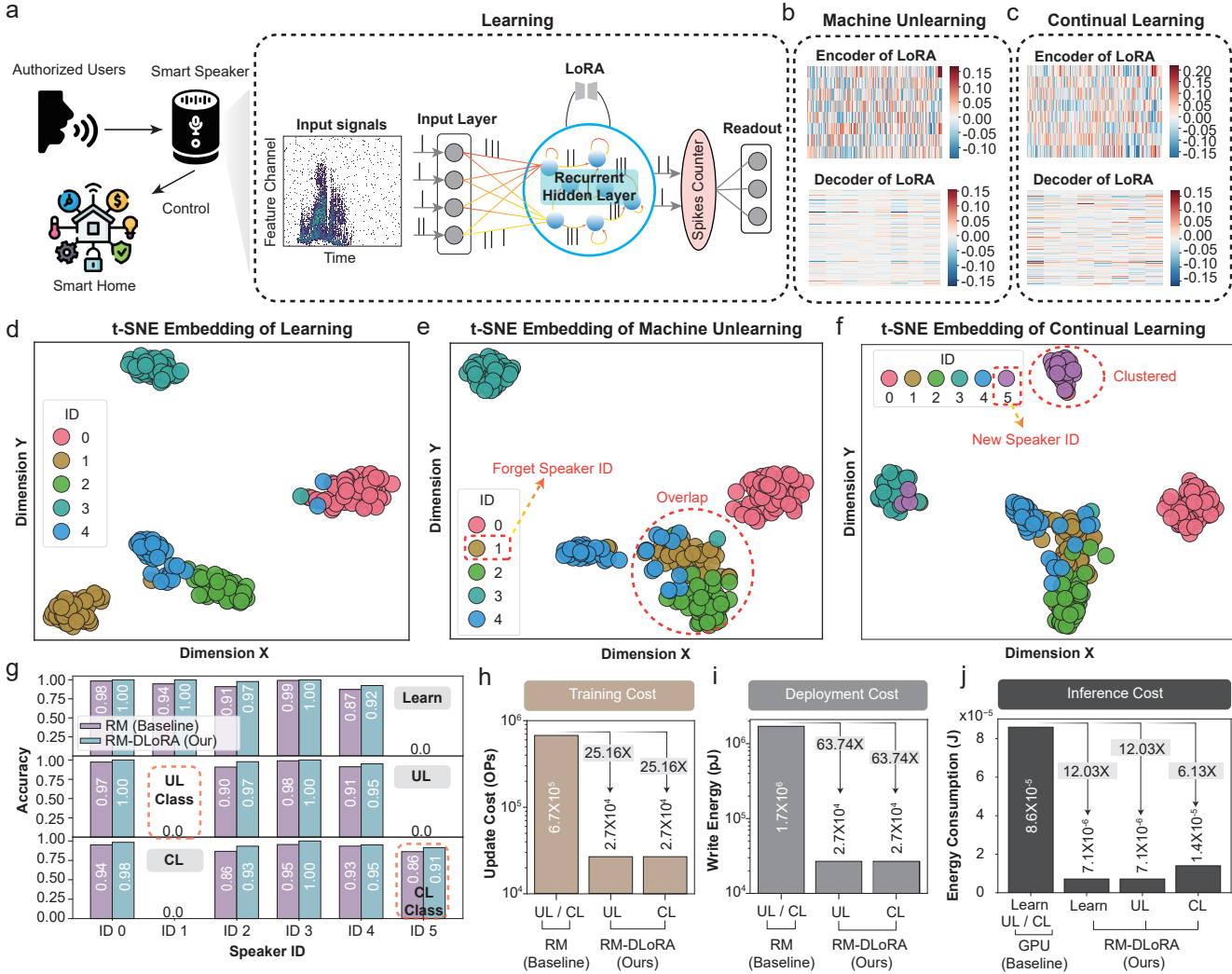


**Figure 4. Learning, machine unlearning and continual learning in an RSNN for speaker-authentication system on the Spiking Speech Commands dataset.** **a**, Schematic of the recurrent spiking neural network (RSNN) architecture. Audio signals from the Spiking Speech Commands dataset are converted into spike trains, accumulated over ten time windows and fed into the recurrent hidden layer of RSNN. **b**, Distributions of LoRA encoder and decoder weights during machine unlearning of speaker ID 1. **c**, Distributions of LoRA encoder and decoder weights during continual learning of a new speaker (ID 5). **d-f**, Two-dimensional t-SNE visualizations of readout-layer activations after learning (**d**), machine unlearning (**e**) and continual learning (**f**). **g**, Per-speaker classification accuracy for RM with digital LoRA updates (RM-DLoRA) and conventional RM program updates, showing that RM-DLoRA mitigates accuracy degradation caused by noise and conductance drift during repeated analogue reprogramming in learn, UL and CL tasks. **h**, Training-update cost for RM-DLoRA and RM by full-parameter fine-tuning, with RM-DLoRA updates reducing the number of training update operations by about  $25.16 \times$  for UL and CL tasks. **i**, Write-energy consumption for RM-DLoRA and RM by full-parameter fine-tuning, with RM-DLoRA updates reducing write energy by about  $63.74 \times$  for UL and CL tasks by avoiding repeated reprogramming of the RM array. **j**, Inference energy for RM-DLoRA and a high-performance GPU, with RM-DLoRA achieving up to  $12.03 \times$  (and at least  $6.13 \times$ ) lower energy consumption across learning (Learn), UL and CL.

Figs. 4a-c illustrate the model architecture and parameter transformations during initial learning, machine unlearning and continual learning in a recurrent spiking neural network (RSNN) architecture inspired by liquid state machine<sup>29</sup> on speaker recognition system. Acoustic inputs are drawn from the Spiking Speech Commands dataset<sup>30</sup>, which contains utterances from many speakers recorded under realistic, less-controlled conditions. As shown in Fig. 4a, raw audio input signals are processed by the input layer and recurrent hidden layer of RSNN for temporal feature extraction, followed by a readout for classification. In the initial learning stage, the pretrained weights of the input, recurrent hidden and readout layers are programmed onto an

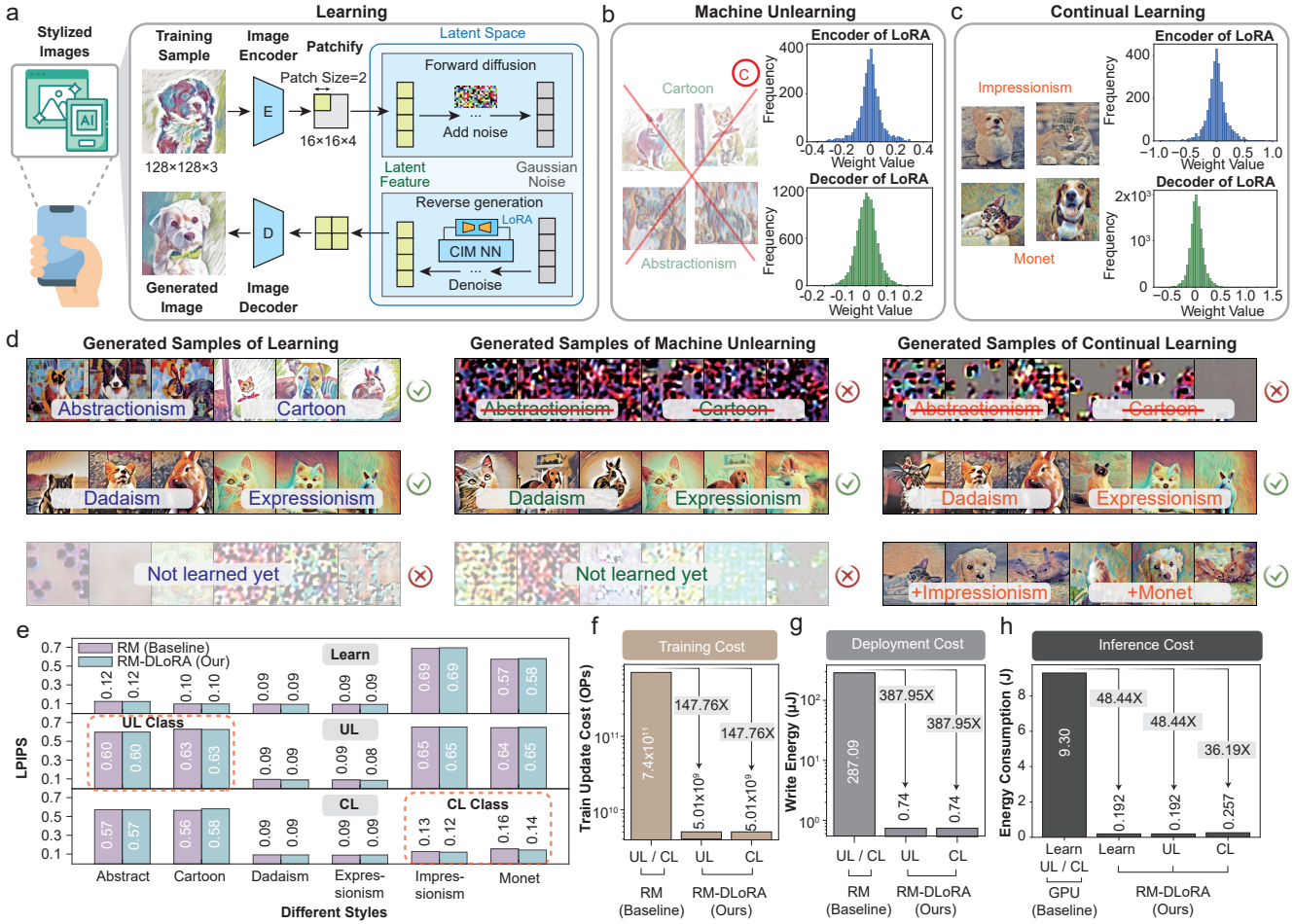


**Figure 5. Learning, machine unlearning and continual learning in a conditional diffusion model on the UnlearnCanvas dataset.** **a**, Architecture of the latent diffusion model. RGB images of size  $128 \times 128 \times 3$  are encoded by a variational autoencoder (VAE) into  $16 \times 16 \times 4$  latent representations, which are partitioned into  $2 \times 2$  patches and fed as latent sequences to a DiT-B/2 backbone. Standard attention layers are replaced by depth-wise convolutional layers to improve efficiency. Image generation is performed by iterative denoising over 100 sampling steps. In the initial learning stage, the model is trained on four artistic styles (Expressionism, Dadaism, Cartoon and Abstractionism). **b**, Machine unlearning of two styles (Cartoon and Abstractionism), revoking the corresponding generative capabilities. **c**, Continual learning of two new styles (Impressionism and Monet), extending the model's repertoire without catastrophic forgetting. **d**, Representative samples generated after learning, machine unlearning and continual learning, showing preservation of image content with appropriate application or suppression of the target styles. **e**, Perceptual generation quality, measured by the Learned Perceptual Image Patch Similarity (LPIPS) metric (lower is better), comparing a full RM program-update baseline and RM-DLoRA; RM-DLoRA achieves comparable quality. **f**, Training update cost across the UL and CL tasks, with RM-DLoRA reducing the number of trainable-parameter updates by about  $147.76 \times$  relative to full-parameter fine-tuning for RM. **g**, Write energy consumption, RM-DLoRA reducing write energy by about  $387.95 \times$  for UL and CL by avoiding repeated analogue reprogramming of the RM array. **h**, Inference energy consumption for RM-DLoRA and a high-performance GPU, showing  $48.44 \times$ ,  $48.44 \times$  and  $36.19 \times$  lower energy for RM-DLoRA across learning (Learn), UL and CL tasks.

RM analog array to support efficient inference. In the subsequent machine unlearning and continual learning processes, the LoRA weights are updated on a digital computer with an SRAM buffer as shown in Figs. 4b and 4c.

Figs. 4d-f present two-dimensional t-SNE visualizations of the readout layer activations after the three stages. After initial learning, activations from five enrolled speakers form distinct, well-separated clusters, indicating accurate speaker discrimination (Fig. 4d). LoRA-based machine unlearning applied to speaker ID 1 causes its former cluster to overlap substantially with those of IDs 2 and 4 (Fig. 4e), reflecting loss of discriminative power for the forgotten speaker while leaving the remaining speakers separable. Subsequent LoRA-based continual learning for a new speaker (ID 5) yields a compact, clearly separated cluster for

the new identity while preserving the separation of the original speakers (Fig. 4f).

Fig. 4g compares inference accuracy across the three tasks (Learn, UL and CL). The RM-DLoRA architecture achieves higher per-speaker accuracy than conventional RM program updates method because it avoids repeated, error-prone analogue reprogramming, thereby reducing cumulative conductance drift in the RM array (see Supplementary Fig. 3 for the noise tolerance of RM programming).

Figs. 4h-j quantify the benefits of the hardware-software co-design for training, on-device deployment and inference. Fig. 4h shows that RM-DLoRA uses substantially fewer trainable parameters than the baseline full-parameter fine-tuning on RM array, reducing the number of training update operations by  $25.16\times$  across UL and CL tasks. Fig. 4i compares write overhead: RM program updates require repeated reprogramming of the entire RM array, whereas our proposed RM-DLoRA updates only the LoRA weights stored in SRAM, reducing write-energy consumption by  $63.74\times$  for UL and CL tasks. As shown in Fig. 4j, the hybrid architecture enables RM-DLoRA to achieve  $12.03\times$ ,  $12.03\times$  and  $6.13\times$  lower inference energy than a high-performance GPU for learning, machine unlearning and continual learning, respectively.

### Stylized Image Generation

Diffusion-based image generation has raised substantial societal concerns, including the creation of harmful content and copyright infringement<sup>31,32</sup>. In such settings, it is often necessary to remove specific generative capabilities. However, privacy and data-security constraints typically preclude access to the original training data, making full retraining from scratch infeasible. Machine unlearning therefore provides a practical approach to selectively eliminating undesired behaviours. Similarly, when diffusion models must be adapted to generate images in new styles or under new conditions, continual learning mechanisms are required to expand model capabilities without catastrophic forgetting.

We demonstrate the effectiveness of our RM-based LoRA framework for initial learning, machine unlearning and continual learning in a conditional diffusion model. Performance is evaluated on the UnlearnCanvas dataset<sup>32</sup>, which focuses on artistic style manipulation, with representative results shown in Fig. 5.

Fig. 5a-c illustrate the model architecture and task sequence. As shown in Fig. 5a, the latent diffusion model takes  $128\times 128\times 3$  input images, which are compressed by a variational autoencoder into  $16\times 16\times 4$  latent representations. These latent maps are tokenized into  $2\times 2$  patches and processed by a DiT-B/2 backbone<sup>33</sup>, in which standard attention layers are replaced with depth-wise convolutions<sup>34</sup> to improve efficiency. The denoising process uses 100 sampling steps during inference to ensure high-quality generation (see Supplementary Fig. 4 for details of the model architecture). In the first phase (Fig. 5b), the model learns four distinct artistic styles (Expressionism, Dadaism, Cartoon and Abstractionism). It then performs targeted machine unlearning of two styles (Cartoon and Abstractionism), mimicking scenarios in which particular generative capabilities must be revoked owing to licensing or ethical constraints. In the continual learning phase (Fig. 5c), the model acquires two new styles (Impressionism and Monet), demonstrating the ability to accumulate new knowledge while retaining prior capabilities.

Representative samples across these stages (Fig. 5d) show that the model preserves content fidelity while correctly applying or suppressing the specified styles. After unlearning, the removed styles no longer appear in generated outputs, providing strict control over prohibited categories (see Supplementary Fig. 5 for additional examples).

Quantitative results corroborate these observations. As shown in Fig. 5e, the full RM program-update baseline achieves perceptual quality that is comparable to our RM-DLoRA method. Perceptual quality is quantified using the Learned Perceptual Image Patch Similarity (LPIPS) metric<sup>35</sup> (lower is better). However, the performance of the full RM program-update baseline degrades severely in the presence of realistic programming noise, whereas RM-DLoRA maintains stable perceptual quality (see Supplementary Fig. 6 for the noise tolerance of RM programming). At the same time, the hybrid RM-DLoRA architecture delivers substantial efficiency gains over full-parameter fine-tuning. Fig. 5f shows reductions in training update cost of  $147.76\times$  for UL and CL tasks, respectively. Fig. 5g reports corresponding write energy savings of  $387.95\times$  for UL and CL tasks reflecting the avoidance of repeated analogue reprogramming of the RM array. Fig. 5h shows that inference energy is reduced by  $48.44\times$ ,  $48.44\times$  and  $36.19\times$  relative to a high-performance GPU for learn, UL and CL tasks, respectively.

## Discussion

This study establishes a hardware-software co-design paradigm for efficient learning, machine unlearning and continual learning, targeting key challenges in secure neuromorphic intelligence. At the hardware level, we propose an analogue-digital hybrid architecture in which the analogue RM array hosts pre-trained weights, while digital computing units implement low-overhead updates for both machine unlearning and continual learning. On the algorithmic side, we exploit low-rank adaptation (LoRA) to confine updates to a small parameter subspace, markedly reducing computational cost and avoiding repeated analogue reprogramming of the RM array.

We demonstrate that this RM-DLoRA framework generalizes across diverse and demanding workloads, including privacy-sensitive face and speaker recognition and conditional diffusion models for stylized image generation. In the discriminative tasks, RM-DLoRA preserves accuracy while reducing training update count and write energy by orders of magnitude relative to

full-parameter fine-tuning on RM, and it achieves substantially lower inference energy than high-performance GPUs, making it well-suited to edge deployment. In the generative setting, evaluated on the UnlearnCanvas dataset, RM-DLoRA supports learning, machine unlearning and continual learning of artistic styles in a conditional diffusion model without degrading perceptual quality, as measured by LPIPS, while delivering large reductions in training, write and inference energy. Critically, targeted machine unlearning revokes specific generative capabilities (for example, prohibited styles), offering a principled route to enforcing privacy, licensing and safety constraints in neuromorphic systems.

## Methods

### Fabrication of RM Chips

The RM chips used in this work comprise a  $32 \times 32$  1T1R array fabricated in a 180 nm CMOS technology node. Each 1T1R cell integrates an access transistor with an RM device formed in the Via4 layer. The RM device stack adopts a TiN/Ta<sub>2</sub>O<sub>5</sub>/TaO<sub>x</sub>/TiN metal-insulator-metal (MIM) structure, with a total switching-layer thickness of 60 nm and top/bottom electrode thicknesses of 40 nm. The array is wired in a standard crossbar configuration with shared word lines (WLs), source lines (SLs) and bit lines (BLs). A post-fabrication annealing step at 400 °C for 30 min in vacuum is applied to improve device-to-device and cycle-to-cycle resistive switching uniformity and endurance.

### Hybrid Analogue-digital Computing System

The hybrid analogue-digital computing system is implemented on a custom printed circuit board (PCB) that integrates the 180 nm RM CIM chip and peripheral circuits, and interfaces to a Xilinx ZC706 evaluation board hosting a Zynq 7000 SoC. The RM macro is addressed via serial-in/parallel-out shift registers (SN74HC595, Texas Instruments) and analogue multiplexers (CD4051B, Texas Instruments), while input voltages are provided by 16-bit digital-to-analogue converters (DAC80508, Texas Instruments). The output currents from the RM array are converted to voltages using transimpedance amplifiers (OPA4322, Texas Instruments) and subsequently digitized by 14-bit analogue-to-digital converters (ADS8324, Texas Instruments), with the digitized data processed by the SoC. A dedicated programming interface connects the RM array to a B1500A semiconductor device analyser for precise conductance initialization and reprogramming.

### Machine Unlearning

Machine unlearning aims to remove the influence of designated training examples from a pretrained model<sup>17</sup>. This is critical for mitigating unintended memorization and leakage of personally identifiable information<sup>36–38</sup>, as well as reducing the generation of unsafe outputs such as toxic or misleading content<sup>20,39–41</sup>. By removing these contributions, unlearning supports compliance with the “right to be forgotten” under privacy-protecting regulations, including the EU General Data Protection Regulation<sup>42</sup> and the California Consumer Privacy Act<sup>43</sup>.

Machine unlearning methods are commonly grouped into *exact unlearning* and *approximate unlearning*<sup>18,19,44</sup>. Exact unlearning retrains the model from scratch after removing the target data, guaranteeing complete erasure but incurring prohibitive computational cost. Approximate unlearning uses more efficient techniques, such as gradient ascent<sup>45</sup> or label obfuscation<sup>44,46</sup>, to approximate the effect of data removal without full retraining.

In this work we focus on efficient realization on RM-based accelerators rather than proposing new unlearning algorithms. We therefore adopt two representative approximate unlearning baselines:

#### Gradient Ascent Based Unlearning

This approach removes the influence of the forget set  $\mathcal{D}_f$  by maximizing its loss, effectively reversing the original gradient descent updates. Starting from the pretrained parameters  $\theta_0$ , the optimization objective is

$$\min_{\theta} \underbrace{-\frac{1}{|\mathcal{D}_f|} \sum_{(x,y_f) \in \mathcal{D}_f} \ell(y_f | x; \theta)}_{\text{gradient ascent on forget set}} + \lambda \underbrace{\frac{1}{|\mathcal{D}_r|} \sum_{(x,y) \in \mathcal{D}_r} \ell(y | x; \theta)}_{\text{gradient descent on retain set}}, \quad (1)$$

where  $\lambda \geq 0$  balances forgetting and retention, and  $\ell(\cdot; \theta)$  denotes the per-sample loss. The negative term induces gradient ascent on  $\mathcal{D}_f$ , pushing predictions away from patterns induced by the forget data, while the retain term preserves performance on the retain set  $\mathcal{D}_r$ .

### Label Obfuscation Based Unlearning

Another widely used technique replaces the original labels of samples in the forget set  $\mathcal{D}_f$  with random incorrect labels and fine-tunes the model on the combined dataset. The optimization objective is

$$\min_{\theta} \underbrace{\frac{1}{|\mathcal{D}_f|} \sum_{(x, \tilde{y}_f) \in \tilde{\mathcal{D}}_f} \ell(\tilde{y}_f | x; \theta)}_{\text{gradient descent on forget set with label obfuscation}} + \lambda \underbrace{\frac{1}{|\mathcal{D}_r|} \sum_{(x, y) \in \mathcal{D}_r} \ell(y | x; \theta)}_{\text{gradient descent on retain set}}, \quad (2)$$

where, for classification tasks,

$$\tilde{\mathcal{D}}_f = \{(x, \tilde{y}_f) \mid (x, y_f) \in \mathcal{D}_f, \tilde{y}_f \sim \text{Uniform}(\mathcal{Y} \setminus \{y_f\})\}, \quad (3)$$

is the forget set with randomized labels  $\tilde{y}_f$ , and  $\lambda \geq 0$ . This encourages the model to treat forgotten samples as belonging to arbitrary incorrect classes, thereby scrambling their original influence while preserving performance on the retain set  $\mathcal{D}_r$ . For other types of tasks, the core idea of this method remains applicable, though its specific form may vary. For example, in generative tasks, when faced with conditions requiring unlearning, the network can be trained to shift its prediction target toward nonsensical or meaningless output.

### Continual Learning

Continual learning methods can be broadly classified into three categories: *regularization-based*<sup>47,48</sup>, *replay-based*<sup>49,50</sup> and *parameter-isolation-based* approaches<sup>47</sup>. These methods update model parameters to accommodate new tasks while preserving prior knowledge. In this work we only focus on efficient deployment on RM-based accelerators, and adopt a *replay-based* continual learning framework as the baseline across all three application scenarios.

Replay-based methods maintain a compact memory buffer of past examples (or generate pseudo-samples) and jointly train them with current-task data to mitigate catastrophic forgetting. Let  $\theta_{t-1}$  denote the model parameters after learning the previous task and  $\ell(\cdot; \theta)$  the per-sample loss. Starting from  $\theta = \theta_{t-1}$ , we optimize the following composite objective,

$$\min_{\theta} \underbrace{\frac{1}{|\mathcal{D}_n|} \sum_{(x, y) \in \mathcal{D}_n} \ell(y | x; \theta)}_{\text{gradient descent on new data}} + \gamma \underbrace{\frac{1}{|\mathcal{D}_p|} \sum_{(x, y) \in \mathcal{D}_p} \ell(y | x; \theta)}_{\text{gradient descent on replay buffer}}, \quad (4)$$

where  $\gamma \geq 0$  controls the trade-off between acquiring new knowledge and retaining prior knowledge,  $\mathcal{D}_n$  denotes the dataset of the current task and  $\mathcal{D}_p$  is the replay buffer storing representative samples from previous tasks (for example, selected via random sampling, herding or gradient-based prioritization). This joint optimization performs gradient descent on both sets, enabling the model to learn new task capabilities from  $\mathcal{D}_n$  while preserving performance on past tasks through  $\mathcal{D}_p$ .

### LoRA-based Machine Unlearning and Continual Learning

To achieve parameter-efficient adaptation in both machine unlearning and continual learning, we incorporate LoRA<sup>26</sup> into the gradient ascent based unlearning and replay-based continual learning frameworks introduced above. LoRA enables efficient fine-tuning by injecting trainable low-rank decomposition matrices into model layers while keeping the pretrained weights  $W_0 \in \mathbb{R}^{d \times k}$  frozen. The updated weight is expressed as

$$W = W_0 + \Delta W = W_0 + BA, \quad (5)$$

where  $B \in \mathbb{R}^{d \times r}$ ,  $A \in \mathbb{R}^{r \times k}$ , and  $r \ll \min(d, k)$  is the rank of the adaptation. Only the low-rank matrices  $A$  and  $B$  are optimized, reducing the number of trainable parameters from  $dk$  to  $r(d + k)$  per layer.

### LoRA-based Machine Unlearning

LoRA substantially reduces the computational and memory overhead of machine unlearning by updating only the LoRA matrices while keeping the pretrained weights  $W_0$  frozen. We apply LoRA to both gradient ascent based and label obfuscation based unlearning baselines, optimizing LoRA parameters  $(A, B)$  (initialized as  $A_0, B_0$ ) such that the forward pass uses the effective weights  $W_0 + BA$ .

**LoRA-based Gradient Ascent Unlearning.** This variant adapts the gradient ascent objective from Equation (1). Optimization is performed solely over the adapter parameters,

$$\min_{A,B} \underbrace{-\frac{1}{|\mathcal{D}_f|} \sum_{(x,y_f) \in \mathcal{D}_f} \ell(y_f | x; W_0 + BA)}_{\text{gradient ascent on forget set}} + \lambda \underbrace{\frac{1}{|\mathcal{D}_r|} \sum_{(x,y) \in \mathcal{D}_r} \ell(y | x; W_0 + BA)}_{\text{gradient descent on retain set}}. \quad (6)$$

The negative term induces gradient ascent on the forget set  $\mathcal{D}_f$  via the adapters, pushing the model away from patterns associated with the data to be forgotten, while the retain term preserves performance on  $\mathcal{D}_r$ . We employ this approach for the face recognition task.

**LoRA-based Label Obfuscation Unlearning.** This method utilizes the label obfuscation Unlearning objective, Equation (2) while training only the adapter parameters,

$$\min_{A,B} \underbrace{\frac{1}{|\mathcal{D}_f|} \sum_{(x,\tilde{y}_f) \in \tilde{\mathcal{D}}_f} \ell(\tilde{y}_f | x; W_0 + BA)}_{\text{gradient descent on forget set with label obfuscation}} + \lambda \underbrace{\frac{1}{|\mathcal{D}_r|} \sum_{(x,y) \in \mathcal{D}_r} \ell(y | x; W_0 + BA)}_{\text{gradient descent on retain set}}, \quad (7)$$

where, for classification tasks,

$$\tilde{\mathcal{D}}_f = \{(x, \tilde{y}_f) \mid (x, y_f) \in \mathcal{D}_f, \tilde{y}_f \sim \text{Uniform}(\mathcal{Y} \setminus \{y_f\})\}, \quad (8)$$

denotes the forget set with randomized incorrect labels  $\tilde{y}_f$ . By fine-tuning only the adapters on this combined dataset, the model effectively erases the influence of the original forget samples while preserving its performance on the retain set. We apply this method to both speaker authentication and stylized image generation.

#### LoRA-based Continual Learning

For replay-based continual learning, LoRA is similarly integrated into the joint training objective in Equation (4). At task  $t$ , we initialize new LoRA adapters ( $A_t, B_t$ ) (or reuse and extend prior adapters) and optimize

$$\min_{A,B} \frac{1}{|\mathcal{D}_n|} \sum_{(x,y) \in \mathcal{D}_n} \ell(y | x; W_0 + BA) + \gamma \frac{1}{|\mathcal{D}_p|} \sum_{(x,y) \in \mathcal{D}_p} \ell(y | x; W_0 + BA). \quad (9)$$

Both terms involve *gradient descent*: the first adapts the model to the new task  $\mathcal{D}_n$ , and the second reinforces prior knowledge via the replay buffer  $\mathcal{D}_p$ . By updating only the LoRA adapters, this technique enables efficient continual learning across face recognition, speaker authentication and stylized image generation tasks without modifying the pretrained weights, mitigating catastrophic forgetting while minimizing resource demands.

## Data Availability

The Olivetti faces dataset<sup>27</sup>, the UnlearnCanvas dataset<sup>32</sup> and Spiking Speech Commands dataset<sup>30</sup> are publicly available.

## Code Availability

The code that supports the plots within this paper is available at <https://github.com/MrLinNing/RMAdaptiveMachine>.

## Acknowledgement

This research is supported by the National Key R&D Program of China (Grant No. 2022YFB3608300), the National Natural Science Foundation of China (Grant Nos. 62374181, 62488101, 62495104), Hong Kong Research Grant Council (Grant No. 17212923, C1009-22G, C7003-24Y and AOE/E-101/23-N). This research is also partially supported by ACCESS - AI Chip Center for Emerging Smart Systems, sponsored by Innovation and Technology Fund (ITF), Hong Kong SAR.

## Author Contributions

N.L., JC.Y., YG.H. contributed to the design and development of the models, software, and hardware experiments. N.L., JC.Y., YG.H., XY.Z., XM.C., DS.S, H.W., XJ.Q., ZR.W. interpreted, analysed and presented the experimental results. All authors discussed the results and implications and commented on the manuscript at all stages.

## Competing Interests

The authors declare no competing interests.

## References

1. Ornes, S. Can neuromorphic computing help reduce ai's high energy cost? *Proc. Natl. Acad. Sci.* **122**, e2528654122 (2025).
2. Indiveri, G. Neuromorphic is dead. long live neuromorphic. *Neuron* (2025).
3. Zhao, R. *et al.* A spiking artificial neuron based on one diffusive memristor, one transistor and one resistor. *Nat. Electron.* 1–11 (2025).
4. Strukov, D. B., Snider, G. S., Stewart, D. R. & Williams, R. S. The missing memristor found. *nature* **453**, 80–83 (2008).
5. Gebregiorgis, A. *et al.* Spike-based neuromorphic computing: An overview from bio-inspiration to hardware architectures and learning mechanisms. *Microprocess. Microsystems* 105240 (2025).
6. Wistuba, M., Sivaprakash, P. T., Balles, L. & Zappella, G. Continual learning with low rank adaptation. *arXiv preprint arXiv:2311.17601* (2023).
7. Jouppi, N. *et al.* Tpu v4: An optically reconfigurable supercomputer for machine learning with hardware support for embeddings. In *Proceedings of the 50th annual international symposium on computer architecture*, 1–14 (2023).
8. Chen, X., Han, Y. & Wang, Y. Communication lower bound in convolution accelerators. In *2020 IEEE International Symposium on High Performance Computer Architecture (HPCA)*, 529–541 (IEEE, 2020).
9. Lanza, M. *et al.* The growing memristor industry. *Nature* **640**, 613–622 (2025).
10. Wan, W. *et al.* A compute-in-memory chip based on resistive random-access memory. *Nature* **608**, 504–512 (2022).
11. Yao, P. *et al.* Fully hardware-implemented memristor convolutional neural network. *Nature* **577**, 641–646 (2020).
12. Liu, K. *et al.* An optoelectronic synapse based on  $\alpha$ -in2se3 with controllable temporal dynamics for multimode and multiscale reservoir computing. *Nat. Electron.* **5**, 761–773 (2022).
13. Rao, M. *et al.* Thousands of conductance levels in memristors integrated on cmos. *Nature* **615**, 823–829 (2023).
14. Song, W. *et al.* Programming memristor arrays with arbitrarily high precision for analog computing. *Science* **383**, 903–910 (2024).
15. Zuo, P. *et al.* Precise and scalable analogue matrix equation solving using resistive random-access memory chips. *Nat. Electron.* 1–12 (2025).
16. Yangdong, X.-J. *et al.* Ultrahigh-precision analog computing using memory-switching geometric ratio of transistors. *Sci. Adv.* **11**, eady4798 (2025).
17. Bourtoule, L. *et al.* Machine unlearning. In *2021 IEEE symposium on security and privacy (SP)*, 141–159 (IEEE, 2021).
18. Liu, S. *et al.* Rethinking machine unlearning for large language models. *Nat. Mach. Intell.* 1–14 (2025).
19. Jia, J. *et al.* Model sparsity can simplify machine unlearning. *Adv. Neural Inf. Process. Syst.* **36**, 51584–51605 (2023).
20. Wu, Y. *et al.* Unlearning concepts in diffusion model via concept domain correction and concept preserving gradient. In *Proceedings of the AAAI Conference on Artificial Intelligence*, 8496–8504 (2025).
21. Park, Y.-H. *et al.* Direct unlearning optimization for robust and safe text-to-image models. *Adv. Neural Inf. Process. Syst.* **37**, 80244–80267 (2024).
22. Kudithipudi, D. *et al.* Design principles for lifelong learning ai accelerators. *Nat. electronics* **6**, 807–822 (2023).
23. Kudithipudi, D. *et al.* Biological underpinnings for lifelong learning machines. *Nat. Mach. Intell.* **4**, 196–210 (2022).
24. Wang, L. *et al.* Incorporating neuro-inspired adaptability for continual learning in artificial intelligence. *Nat. Mach. Intell.* **5**, 1356–1368 (2023).
25. Van de Ven, G. M., Tuytelaars, T. & Tolias, A. S. Three types of incremental learning. *Nat. Mach. Intell.* **4**, 1185–1197 (2022).
26. Hu, E. J. *et al.* Lora: Low-rank adaptation of large language models. In *International Conference on Learning Representations* (2022).

27. Samaria, F. S. & Harter, A. C. Parameterisation of a stochastic model for human face identification. In *Proceedings of 1994 IEEE workshop on applications of computer vision*, 138–142 (IEEE, 1994).
28. Tolstikhin, I. O. *et al.* Mlp-mixer: An all-mlp architecture for vision. *Adv. neural information processing systems* **34**, 24261–24272 (2021).
29. Lin, N. *et al.* Resistive memory-based zero-shot liquid state machine for multimodal event data learning. *Nat. Comput. Sci.* **5**, 37–47 (2025).
30. Cramer, B., Stradmann, Y., Schemmel, J. & Zenke, F. The heidelberg spiking data sets for the systematic evaluation of spiking neural networks. *IEEE Transactions on Neural Networks Learn. Syst.* **33**, 2744–2757 (2020).
31. Tsai, Y.-L. *et al.* Ring-a-bell! how reliable are concept removal methods for diffusion models? *arXiv preprint arXiv:2310.10012* (2023).
32. Zhang, Y. *et al.* Unlearn canvas: A stylized image dataset to benchmark machine unlearning for diffusion models. *CoRR* (2024).
33. Peebles, W. & Xie, S. Scalable diffusion models with transformers. In *Proceedings of the IEEE/CVF international conference on computer vision*, 4195–4205 (2023).
34. Liu, Z. *et al.* A convnet for the 2020s. In *Proceedings of the IEEE/CVF conference on computer vision and pattern recognition*, 11976–11986 (2022).
35. Zhang, R., Isola, P., Efros, A. A., Shechtman, E. & Wang, O. The unreasonable effectiveness of deep features as a perceptual metric. In *Proceedings of the IEEE conference on computer vision and pattern recognition*, 586–595 (2018).
36. Fredrikson, M., Jha, S. & Ristenpart, T. Model inversion attacks that exploit confidence information and basic countermeasures. In *Proceedings of the 22nd ACM SIGSAC conference on computer and communications security*, 1322–1333 (2015).
37. Carlini, N., Liu, C., Erlingsson, Ú., Kos, J. & Song, D. The secret sharer: Evaluating and testing unintended memorization in neural networks. In *28th USENIX security symposium (USENIX security 19)*, 267–284 (2019).
38. Carlini, N. *et al.* Extracting training data from large language models. In *30th USENIX security symposium (USENIX Security 21)*, 2633–2650 (2021).
39. Kumari, N. *et al.* Ablating concepts in text-to-image diffusion models. In *Proceedings of the IEEE/CVF International Conference on Computer Vision*, 22691–22702 (2023).
40. Zhang, Y. *et al.* To generate or not? safety-driven unlearned diffusion models are still easy to generate unsafe images... for now. In *European Conference on Computer Vision*, 385–403 (Springer, 2024).
41. Zhang, Y. *et al.* Defensive unlearning with adversarial training for robust concept erasure in diffusion models. *Adv. neural information processing systems* **37**, 36748–36776 (2024).
42. Mantelero, A. The eu proposal for a general data protection regulation and the roots of the ‘right to be forgotten’. *Comput. Law & Secur. Rev.* **29**, 229–235 (2013).
43. Chau. Assembly bill no. 375: An act to add title 1.81.5 (commencing with section 1798.100) to part 4 of division 3 of the civil code, relating to privacy (2018). California Consumer Privacy Act of 2018 (Chapter 55, Statutes of 2018).
44. Xu, H., Zhu, T., Zhang, L., Zhou, W. & Yu, P. S. Machine unlearning: A survey. *ACM Comput. Surv.* **56**, DOI: [10.1145/3603620](https://doi.org/10.1145/3603620) (2023).
45. Liu, Y. *et al.* Backdoor defense with machine unlearning. In *IEEE INFOCOM 2022-IEEE conference on computer communications*, 280–289 (IEEE, 2022).
46. Graves, L., Nagisetty, V. & Ganesh, V. Amnesiac machine learning. In *Proceedings of the AAAI Conference on Artificial Intelligence*, 11516–11524 (2021).
47. De Lange, M. *et al.* A continual learning survey: Defying forgetting in classification tasks. *IEEE transactions on pattern analysis machine intelligence* **44**, 3366–3385 (2021).
48. Van de Ven, G. M., Siegelmann, H. T. & Tolias, A. S. Brain-inspired replay for continual learning with artificial neural networks. *Nat. communications* **11**, 4069 (2020).
49. Rebuffi, S.-A., Kolesnikov, A., Sperl, G. & Lampert, C. H. icarl: Incremental classifier and representation learning. In *Proceedings of the IEEE conference on Computer Vision and Pattern Recognition*, 2001–2010 (2017).
50. Shin, H., Lee, J. K., Kim, J. & Kim, J. Continual learning with deep generative replay. *Adv. neural information processing systems* **30** (2017).